JOURNAL OF CATALYSIS 136, 161–169 (1992)

Electronic Interaction between Supports and Ruthenium Catalysts for the Hydrogenation of Carbon Monoxide

TATSUMI ISHIHARA,[1] KAZUAKI HARADA, KOICHI EGUCHI, AND HIROMICHI ARAI[2]

Department of Materials Science and Technology, Graduate School of Engineering Sciences, Kyushu University, Kasuga-shi, Fukuoka 816, Japan

Received March 8, 1990; revised November 4, 1991

The effect of oxide supports in hydrogenation of CO was investigated using Ru supported on metal oxides as catalysts. Activity for CO hydrogenation and product distribution depended on the electron affinity of the oxide supports. A support effect was also recognized in the adsorption state of hydrogen and carbon monoxide from temperature-programmed desorption (TPD) experiments. The support effect observed in this study seems to result from electronic interaction between Ru and support oxide, since the binding energy of Ru $3d_{5/2}$ XPS peaks and the IR absorption frequency of linear-type NO depended on the electron affinity of the oxide support. The extent of charge transfer was represented by the electronegativity of support oxide in this study. The activity and the chain growth probability in CO hydrogenation are enhanced by using Ru on support oxides with high electronegativity because the deficient electron density of Ru weakened the CO adsorption and enhanced the concentration of hydrogen on catalyst surface.

INTRODUCTION

Recent publications on supported metal catalysts have revealed that the support oxides have chemical influences on the activity of metal catalysts. Particular interest has been focused on the use of reducible supports such as TiO_2 or Nb_2O_5 (*1*). After the report on metal-support interaction by Tauster *et al.* (*2, 3*), many researchers reported the reduced chemisorption capacity of CO and H_2 due to a strong interaction between Group VIII metals and support oxide, such as TiO_2, but the support effects under a "non-SMSI" state are not clarified satisfactorily. The high catalytic activity of TiO_2-supported catalyst for CO hydrogenation was pointed out and investigated by many researchers (*4*). The support effects are sometimes caused by charge transfer between support and metal (*5, 6*) or sometimes by new active sites created at the interface between metal and a support oxide (*7, 8*). In particular, electronic metal–support interaction becomes influential when there are small metal crystallites. Kao *et al.* (*9*) have reported from XPS measurements on a Ni/TiO_2 [110] model catalyst that about 0.1 electron per Ni atom transfers from TiO_2 to Ni. Recently X-ray absorption studies have shown that the support oxide can have a marked effect on the electron density of the metal (*10*). From a comparison of the X-ray absorption near-edge structure (XANES) of Rh/TiO_2 and Rh metal, Reasco *et al.* (*10*) reported that the average electronic environment of the Rh in Rh/TiO_2 changes from that of Rh metal as a result of the net electron transfer from TiO_2 to Rh catalyst. Electron spectroscopic studies on Rh films on a TiO_2 (110) surface also establish that there is electron transfer from the reduced TiO_2 surface to the Rh film (*11*). In the present study, we tried to investigate statistically the support effect on Ru catalyst hydrogenation in relation to the adsorption properties of CO and H_2 when the metal was supported on 19 different kinds of metal oxides.

[1] Present address: Faculty of Engineering, Oita University, Oita, 870-11, Japan.

[2] To whom correspondence should be addressed.

0021-9517/92 $5.00

EXPERIMENTAL

Catalyst Preparation

The supported Ru catalysts, except for Ru/CaO, Ru/MgO, and Ru/zeolite, were prepared by the incipient wetness technique using $RuCl_3$ aqueous solution. Impregnation to CaO or MgO was carried out in acetone solution of $RuCl_3$ to avoid the formation of Mg or Ca chlorides. Ru/zeolite was prepared by ion exchange with $[Ru(NH_3)_6]Cl_3$ aqueous solution (0.1 mol/l). Ruthenium loading was 2 wt.% in every case. The supported Ru samples thus obtained were reduced at 673 K for 4 h in a hydrogen stream. The phase of oxide supports was identified by X-ray diffraction after preparation; however, no diffraction peaks from Ru metal were detected because of its small particle size.

Apparatus and Procedure

Catalytic hydrogenation of CO was performed in a high pressure flow system with a fixed bed reactor. Catalysts were preheated in a hydrogen stream at 523 K for 1 h before reaction. A gaseous mixture of H_2 (62 vol%), CO (33 vol%), and Ar (5 vol%), which was freed of water and carbonyl impurities by active alumina and 13X-type zeolite, was fed to the catalyst bed at $W/F = 10$ g-cat h/mol, where W is the catalyst weight and F the total flow rate. Unless otherwise noted, the reaction data were taken at 523 K and at 1.0 MPa. Products were analyzed by gas chromatography as previously described (*12*). The product selectivities are expressed on the basis of related CO.

The XPS studies were carried out with a VG Scientific ESCA-3 Mark II spectrometer after reduction at 673 K. The binding energy of the Ru $3d_{5/2}$ peak was corrected by comparing the Au $4f_{5/2}$ peaks on the sample with that of Au foil.

Electron microscopic observation was carried out with a JEOL JEM-1000 instrument at an acceleration voltage of 1000 kV. Particle size distribution was estimated by observation on about a hundred Ru particles on the same support oxide. It was confirmed that Ru particles larger than 10 nm did not exist on any support oxides from observation under low magnification.

Temperature-programmed desorption (TPD) of hydrogen or carbon monoxide was carried out in a flow system (*12*). Catalysts (ca. 0.2 g) were heated in H_2 at 673 K for 1 h and subsequently in Ar at 973 K for 10 min. Hydrogen or carbon monoxide was adsorbed on the catalysts at 673 K and then evacuated at room temperature. Purified argon and helium were used as the carrier gases for TPD of H_2 and CO, respectively. Impurity oxygen in these commercial gases was removed by an electrochemical oxygen pump using yttria-stabilized zirconia (YSZ) as an electrolyte. During heating in a programmed schedule (9 K/min), desorption of hydrogen or carbon monoxide from the sample was monitored by two thermal-conductivity detectors (TCD). Water and carbon dioxide were removed with a cold trap which was placed between the detectors.

In situ infrared spectra were recorded with a JASCO IR-1A spectrometer. A sample disk was heated at 673 K for 3 h *in vacuo* to remove water and other adsorbed gases. Nitrogen monoxide was introduced to the sample at room temperature and heated up to 423 K. After adsorption, NO in the gas phase was evacuated at room temperature prior to the IR measurements. The background spectrum of the catalyst without adsorption treatment was subtracted from the measured spectra after NO adsorption.

RESULTS

Particle Size Distribution

The particle sizes of the supported Ru were obtained by electron microscopic observation as shown in Fig. 1. Due to low electron transmission, ruthenium particles on the support could only be observed for six kinds of support oxide. The particle size of Ru on the HY support was small enough to be present in the pores of the support (1

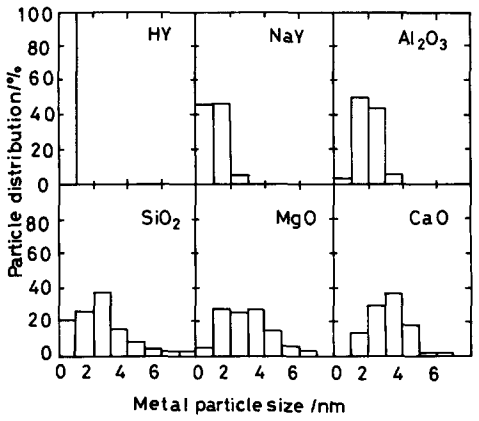

FIG. 1. Particle size distribution of supported Ru catalyst.

nm in diameter), but those on MgO, SiO_2, and CaO were widely distributed between 1 nm and 10 nm. The average particle sizes were smaller than 2 nm on HY and NaY supports.

Hydrogenation of Carbon Monoxide

The activities and the product distributions over the supported Ru catalysts are summarized in Table 1. Hydrocarbon products are grouped into four categories, i.e., CH_4, C_2–C_4 paraffins, C_2–C_4 olefins, and hydrocarbons with five or more carbon atoms (C_{5+}). Formation of carbon dioxide was negligible on every catalyst.

The catalytic activity and product distributions strongly depended on the kind of oxide support. High dispersion of Ru as with Ru/HY did not always result in high CO conversion. The conversions of CO were relatively high on Ru/ZrO_2, Ru/Nb_2O_5, and Ru/SiO_2. Ru/V_2O_3 was the most active among the catalysts in Table 1. Small amounts of the oxygenated compounds, mainly methanol, were formed on some catalysts. The selectivity to oxygenated compounds in this study was the highest on Ru/SiO_2. Methanation was dominant on Ru/SiO_2 and Ru/ZrO_2. The activities were

TABLE 1

Activity and Selectivity of CO Hydrogenation over Ru Supported on Various Oxides

Support	CO conv. (%)	T.O.F.	Selectivity (%)					
			CH_4	$C_2^=$–$C_4^=$	C_2^-–C_4^-	C_{5+}	Oxy.	CO_2
CaO	3.0	0.48	50.2	45.2	4.6	0	0	0
MgO	5.4	0.35	33.0	29.3	14.9	17.8	0	5.0
La_2O_3	4.2	0.27	41.1	32.4	3.7	18.9	0	3.9
ZnO	6.5	0.92	14.6	36.5	12.1	36.8	0	0
CeO_2	11.5	1.58	13.7	27.0	12.9	45.5	0.9	0
Al_2O_3	37.6	1.52	19.4	20.3	13.3	44.4	3.0	0
MnO_2	22.1	9.16	12.4	25.6	10.3	49.5	1.2	0
Cr_2O_3	9.5	1.72	21.9	16.1	6.2	55.8	0	0
V_2O_3	63.9	7.23	12.6	15.9	21.5	44.6	0	0
ZrO_2	41.9	3.42	24.9	24.2	15.9	35.0	0	0
TiO_2	31.9	2.60	19.5	19.5	13.3	45.0	2.7	0
Nb_2O_5	39.8	10.09	17.9	14.8	11.1	56.2	0	0
MoO_3	12.3	15.20	22.7	16.8	14.0	41.6	1.7	3.2
SiO_2	38.2	4.15	49.1	7.8	12.6	27.0	3.5	0
NaY	24.5	0.66	15.8	16.3	13.8	54.1	0	0
HY	15.5	0.40	29.2	12.7	21.1	35.0	0	2.0

Note. $C_2^=$–$C_4^=$: C_2–C_4 olefins; C_2^-–C_4^-: C_2–C_4 paraffin; C_{5+}: hydrocarbons with five or more carbon atoms, Oxy.: oxygenated compounds; T.O.F.: turnover number on the basis of CO uptakes; Reaction conditions: 523 K, 1.0 MPa, W/F = 10 g-cat h/mol, H_2/CO = 2.

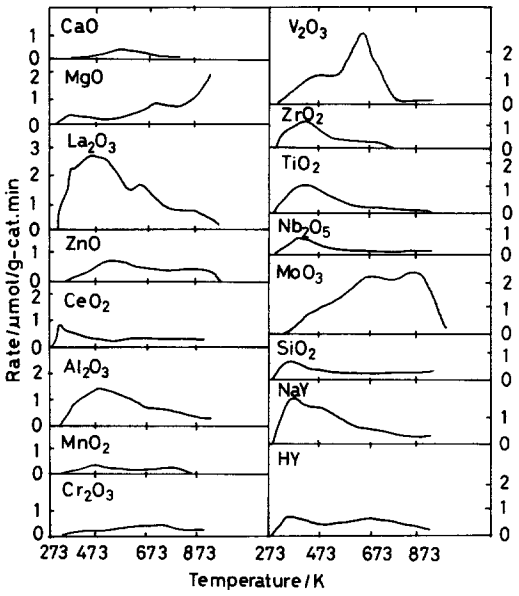

FIG. 2. TPD curves of H_2 from supported Ru catalysts. H_2 adsorption 673–298 K, heating rate 9 K/min.

generally low on Ru catalyst supported on electron-donating oxides, such as CaO, MgO, and ZnO.

Temperature-Programmed Desorption of CO and H_2

The effect of the support on the adsorption states was examined by the thermal desorption of hydrogen and carbon monoxide (Fig. 2). Desorption profiles of hydrogen from Ru catalysts strongly depend upon the kind of oxide support. Hydrogen desorbed above 473 K from Ru/CaO and Ru/MgO but below 473 K from Ru/SiO_2. These differences in H_2 desorption temperature are closely related to the CO hydrogenation activity, as will be discussed below. A large amount of hydrogen, about twice as large an amount as that of the supported Ru, desorbed from Ru/V_2O_3 and Ru/MoO_3. This implies that hydrogen spill-over may occur on Ru/V_2O_3 and Ru/MoO_3 (*13*).

Desorption curves of CO from various Ru catalysts are shown in Fig. 3. The adsorption state of CO also strongly depended on the oxide support. A large amount of CO_2 desorbed from Ru/CaO and Ru/MgO. The adsorption of CO appears to be so strong that the disproportionation of adsorbed CO proceeded dominantly on Ru supported on CaO and MgO. On the other hand, the amount of CO_2 desorption was negligibly small from Ru on support oxides such as ZnO, MnO_2, and Cr_2O_3. The adsorption state of H_2 and CO appears to sensitively reflect the state of Ru catalyst.

IR Measurements

Infrared spectroscopy of adsorbed NO is effective in elucidating the electronic state of metals, as has been reported previously (*14*). A strong N–O stretching band appeared in the IR spectrum of every catalyst in the range of 1860 to 1890 cm^{-1} after NO adsorption and its absorption frequency depended on the kinds of support (Fig. 4). Nitrogen oxide adsorbs on the metal surface as three types, i.e., NO^+, NO, and NO^- (*15*). Since absorbances of the infrared peak

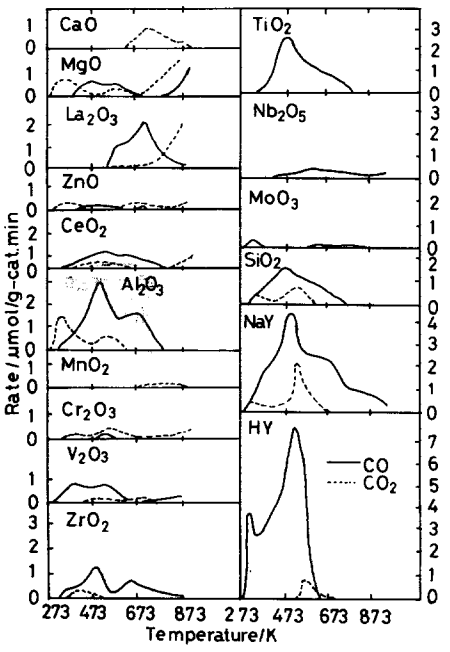

FIG. 3. TPD curves of CO from supported ruthenium catalysts. CO adsorption 673–298 K, heating rate 9 K/min.

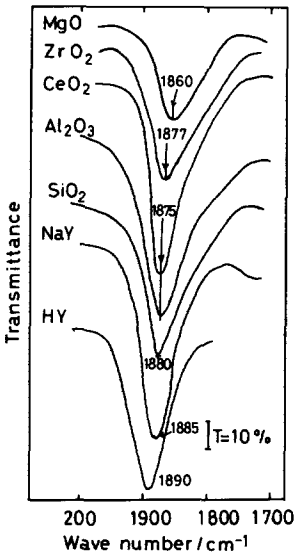

FIG. 4. IR spectra of adsorbed NO on supported Ru catalysts.

at 1860–1890 cm^{-1} are unchanged by elevating temperature in oxygen, these absorption bands can be assigned to the adsorption of linear type (NO^+) (*15*).

XPS Measurements

The corrected binding energies of Ru $3d_{5/2}$ are summarized in Table 2. XPS studies were carried out just after the reduction at 673 K. Therefore, the high-vacuum atmosphere during XPS measurement seems not to have a serious effect on the oxidation state of the support because the atmosphere for reduction is more severe in a hydrogen stream at 673 K than in the high-vacuum atmosphere during XPS measurement. It is apparent that the binding energy of Ru is affected by the support oxide. The binding energy of Ru $3d_{5/2}$ is low on Al_2O_3, while it is high on NaY and HY. This shift in binding energy suggests that charge transfer from Ru to support oxide is brought about, as discussed below.

TABLE 2

Binding Energy of Ru $3d_{5/2}$ Peaks on Supported Ru Catalyst

Support	Binding energy of Ru $3d_{5/2}$ (eV)	Support	Binding energy of Ru $3d_{5/2}$ (eV)
Al_2O_3	280.1	TiO_2	280.3
Nb_2O_5	280.5	SiO_2	280.7
NaY	280.9	HY	280.9

DISCUSSION

The remarkable support effects observed on the catalytic activity might partly result from the particle size of the metal. Metal dispersion is estimated from the TEM observation and the amount of adsorbed hydrogen and carbon monoxide as summarized in Table 3. Although the particle size estimated from H_2 adsorption is sometimes larger than that from the TEM observation and CO adsorption amount, the particle size estimated from the three methods is virtually consistent. It should also be noted that removing Cl^- by reduction is difficult (*16*). The amount of adsorbed CO is often greater than that of H_2 because residual Cl^- appears to reduce the amount of H_2 adsorption (*17*). Activity, selectivity, and also the adsorption behavior of Ru catalysts are independent of the particle size because no relationship can be recognized between Ru particle size and activity or selectivity by comparing with Tables 1 and 3. In particular, the particle size distribution of Ru/SiO_2, Ru/MgO, and Ru/CaO were almost similar as observed by the TEM observation in Fig. 1, while they are largely different in CO hydrogenation activity, product distribution, and adsorption properties. This suggests that the variation in the catalytic and adsorption behavior of supported Ru catalysts is more strongly influenced by chemical interaction between the support and Ru than by the variation in particle size of Ru.

Three possibilities are considered as chemical interactions between support and Ru, namely (i) an electronic interaction, (ii) creation of active sites at the interface of metal and oxide support, and (iii) a decrease in surface area of Ru due to migration of reduced support oxide. Migration of re-

TABLE 3

Particle Size of Ru Estimated from TEM Observation and from H_2 and CO Uptakes

Support	Surface area ($m^2\ g^{-1}$)[a]	Particle size (nm)[b]	H_2 adsorption[c]			CO adsorption[d]		
			Uptake ($\mu mol\ g^{-1}$)	H/Ru	Particle size (nm)	Uptake ($\mu mol\ g^{-1}$)	CO/Ru	Particle size (nm)[e]
CaO	14.0	3.28	12.3	0.12	9.0	33.8	0.17	6.4
MgO	96.3	3.21	26.1	0.25	3.4	83.7	0.42	2.6
La_2O_3	10.4	[f]	74.2	0.75	1.5	85.4	0.43	2.5
ZnO	19.3	[f]	18.1	0.32	6.0	38.9	0.20	5.6
CeO_2	3.8	[f]	17.0	0.33	6.4	40.0	0.20	4.9
Al_2O_3	193.0	1.60	55.0	0.55	2.0	135.7	0.69	1.6
MnO_2	25.4	[f]	11.1	0.11	9.7	13.3	0.06	16.3
Cr_2O_3	3.0	[f]	15.6	0.16	6.9	30.4	0.15	7.1
V_2O_3	4.0	[f]	51.2	0.52	2.1	48.6	0.25	4.4
ZrO_2	10.8	[f]	32.4	0.48	3.3	67.4	0.34	3.2
TiO_2	59.2	[f]	41.6	0.56	2.6	67.5	0.34	3.2
Nb_2O_5	8.0	[f]	18.2	0.29	5.9	21.7	0.11	10.0
MoO_3	19.8	[f]	70.5	0.71	1.5	4.5	0.02	48.5
SiO_2	316.0	3.58	27.2	0.27	3.7	50.0	0.25	3.4
NaY	720.0	1.11	46.1	0.46	2.8	204.8	1.03	1.1
HY	716.0	0.81	29.4	0.29	3.9	212.0	1.08	1.0

[a] BET surface area of support oxide.
[b] Estimated by the TEM observation.
[c] Desorption amount in H_2-TPD.
[d] Desorption amount in CO-TPD.
[e] Calculated by assuming that CO adsorbs on Ru stoichiometrically.
[f] Particle size could not be estimated with TEM observation due to low electron transmission.
NaY: NaY-type zeolite; HY: HY-type zeolite.

duced oxide on Ru surface is not likely to have occurred in this study because of the low reduction temperature. It is reported that migration of reduced support oxide occurs during heat treatment above 773 K (*2, 3*). On the other hand, electronic metal–support interaction becomes influential for small metal crystallites less than 5 nm in size (*18*). The binding energy of Ru $3d_{5/2}$ depended on the oxide support (Table 2). A binding energy shift is sometimes caused by a particle size effect, e.g., for Pt/TiO_2, an increase in binding energy was observed with increasing metal dispersion (*19*). The binding energy of Ru $3d_{5/2}$, however, is independent of particle size (Table 2). The present results can be explained by an electronic interaction due to the electron-donating or electron-accepting properties of oxide support. The electron-donating oxides such as MgO or CaO suppressed the CO hydrogenation activity. On the other hand, the electron-accepting oxides such as SiO_2, Nb_2O_5, and MoO_3 enhanced the hydrogenation activity and increased the chain growth probability.

The electronegativity of an oxide is a measure of its electron affinity (*20*). In this study, we take the electron-attractive property of an oxide to be represented by the electronegativity of the oxide based on the Sanderson concept (*21*). This is because the electronegativity of elements is shifted in an intermediate direction in compounds when elements with differing electronegativity are bonded chemically. The geometric mean of the electronegativities of the elements in an oxide is defined as the electronegativity of

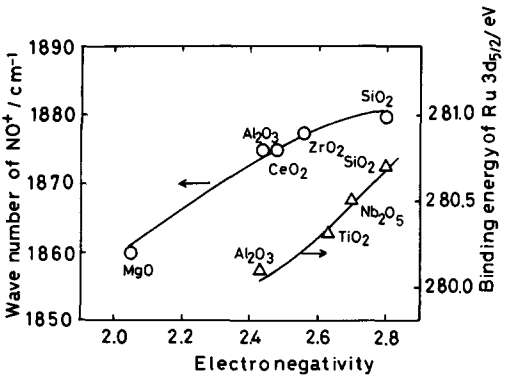

FIG. 5. Adsorption frequency of linear type NO and binding energy of Ru $3d_{5/2}$ as a function of the electronegativity of support oxide: (○) Absorption frequency of NO^+, (△) binding energy of Ru $3d_{5/2}$.

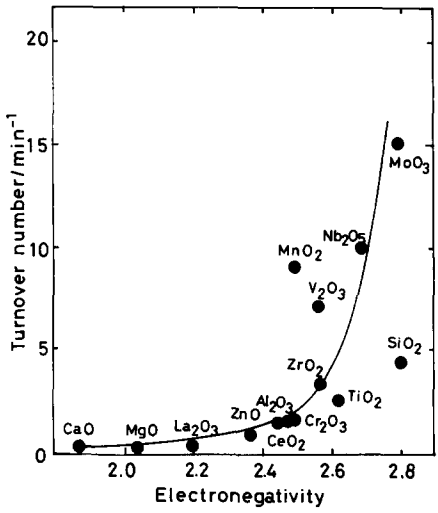

FIG. 6. Correlation between turnover number and electronegativity of oxide supports.

the oxide by Sanderson (*21*). The electronegativity for the element defined by Pauling is used for the calculation of the electronegativity of oxides (*22*). Some of the reducible oxides such as TiO_2 and MnO_2 may be partially reduced during hydrogen treatment, but partially reduced oxide could not be detected by X-ray diffraction or XPS after H_2 reduction at 673 K. Since it is expected that the amount of partially reduced oxide is not large, the electronegativity of the oxide was calculated by neglecting the partial reduction of support oxide during reduction. IR spectra of adsorbed NO also suggest that there is charge transfer beween metal and oxide support depending on the electronegativity of oxide. Only linear-type (NO^+) was recognized on the supported Ru catalysts. The absorption frequency of linear-type NO shifted to a higher wavenumber with increasing electronegativity of oxide supports as shown in Fig. 5. The higher shift in wavenumber of the NO^+ band is caused by increasing the electron donation from adsorbed NO to Ru (*23*). The binding energy of the Ru $3d_{5/2}$ peak was also shifted to higher energy with increasing electronegativity of support oxide (Fig. 5). The shifts in the wavenumber of adsorbed NO and the binding energy of Ru $3d_{5/2}$ confirm that the electron density of Ru decreases with increasing electronegativity of the oxide support as a result of the electronic interaction between metal and support oxide. The amounts of H_2 and CO adsorbed on the metal and their relative ratio (H_2/CO) should be affected by the electron density of Ru.

The turnover number and the chain growth probability are plotted as a function of the electronegativity of the support oxides in Figs. 6 and 7. Since the CO uptake

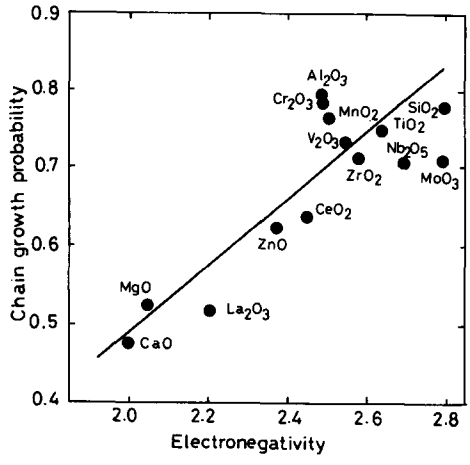

FIG. 7. Correlation between chain growth probability and electronegativity of oxide supports.

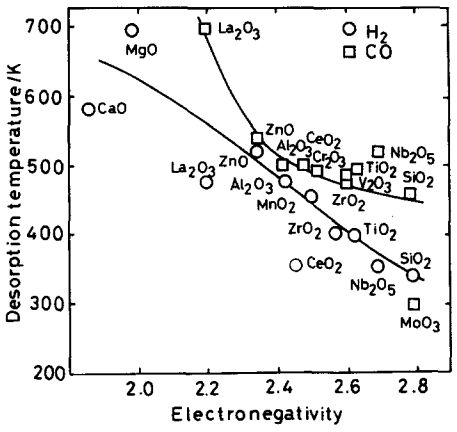

FIG. 8. Desorption temperature of H_2 and CO as a function of electronegativity of support oxide.

corresponds well with the metal surface area (Table 3), turnover number in this study is obtained on the basis of CO uptakes. The turnover number and the chain growth probability are small over Ru supported on the oxides with low electronegativity, but tend to increase with increasing electronegativity of support oxides (Figs. 6 and 7). Formation of paraffin was promoted on oxide supports with high electronegativity. As discussed above, partial reduction of the support oxide is negligible in this study. However, it is expected that some of the reducible oxides such as TiO_2 and MnO_2 did partially reduce under CO hydrogenation. The deviation of the points for some catalysts such as MnO_2 may result from such partial reduction of the support oxide. Thus, the electron affinity of the oxide appears to control the catalytic activity and selectivity of Ru for CO hydrogenation.

The temperatures at the maximum rates of H_2 and CO desorption in the TPD experiments are plotted as a function of the electronegativity of the support oxide in Fig. 8. Temperature in Fig. 8, therefore, reflects the strength of the chemical bonds between the metal and hydrogen or carbon monoxide. Hydrogen desorbed above 673 K from Ru on the electron-donating oxides, but below 473 K from Ru on the electron-accepting oxides. The low temperature desorption of H_2 became dominant as the electronegativity of the oxide increased in Fig. 8. The lower shift in hydrogen desorption temperature may result from the low electron density of Ru as discussed above. On the other hand, a large amount of CO_2 desorbs from Ru on oxide supports with low electronegativity. Disproportionation of CO is known to be promoted by addition of K to Ru/SiO_2 (*24*). Dissociative adsorption and disproportionation of CO is facilitated because of the high electron density of Ru. The increase of electron donation from Ru to CO by K addition promotes the dissociation of C–O bond by analogy with the oxide supports with low electronegativity. The desorption temperature of CO at maximum rate is also plotted versus the electronegativity of support oxide in Fig. 8. The points of Ru/MgO and Ru/CaO were excluded from the plot because the dissociative adsorption of CO is dominant. Since the desorption temperature of CO shifted to lower temperature, adsorption of CO is weakened with increasing electronegativity of oxide. The catalyst surface appears to be covered with CO on Ru supported on oxide with low electronegativity because the adsorption of CO is much stronger than that of H_2 in Fig. 8. Such catalysts are inactive for CO hydrogenation because hydrogen chemisorption is strongly inhibited. The inhibition of H_2 chemisorption by CO adsorption was also reported on Ni catalysts (*25*). On the other hand, the desorption measurement suggests that the strength of CO adsorption is approximately equal to that of hydrogen on Ru supported on oxide with high electronegativity (Fig. 8). Weakening CO adsorption may provide sites for hydrogen adsorption. The high concentration of adsorbed hydrogen on Ru on the support oxides with high electronegativity resulted in a high CO hydrogenation activity and high chain growth probability. Adsorption strength of CO or H_2 seems to be related to the electron density in Ru through the interaction with support oxide.

CONCLUSION

The catalytic behavior of Ru for CO hydrogenation is strongly affected by the support material. Appropriate selection of support materials is necessary not only to provide a large reaction surface, but also to attain excellent catalyst performance due to the effect of metal–support interaction. In particular, the electron-accepting or electron-donating property of support oxides is one of the important factors in the present work with Ru catalysts, because the small deviation of electron density from the neutral state of Ru strongly affects the adsorption strength of H_2 and CO on the Ru surface. Control of the electronic state of the metal by metal–support interaction, e.g., by addition of acidic or basic reagents or by mixing support oxides, may be a promising way to improve the performance of Ru catalysts.

REFERENCES

1. Ko, E. I., Bafrali, R., Nuhfer, N. T., and Wagner, N. J., *J. Catal.* **95,** 260 (1985).
2. Tauster, S. J., and Fung, S. C., *J. Catal.* **55,** 29 (1978).
3. Tauster, S. J., Fung, S. C., Garten, R. L., *J. Am. Chem. Soc.* **100,** 170 (1978).
4. McVicker, G. B., and Ziemiak, J. J., *J. Catal.* **95,** 473 (1985).
5. Herrmann, J. M., *J. Catal.* **89,** 404 (1984).
6. Fung, S. C., *J. Catal.* **76,** 225 (1982).
7. Bracey, J. B., and Burch, R., *J. Catal.* **86,** 384 (1984).
8. Zhao, Y. B., and Chung, Y. W., *J. Catal.* **106,** 369 (1987).
9. Kao, C. C., Tsai, S. C., and Chung, Y. W., *J. Catal.* **73,** 136 (1982).
10. Resasco, D. E., Weber, R. S., Sakellson, S., McMillan, M., and Haller, G. L., *J. Phys. Chem.* **92,** 189 (1988).
11. Sadeghi, H. R., and Henrich V. R., *J. Catal.* **109,** 1 (1988).
12. Ishihara, T., Eguchi, K., and Arai, H., *Appl. Catal.* **30,** 225 (1987).
13. Conner, W. C., Pajonk, G. M., and Teichner, S. J., *Adv. Catal.* **34,** 1 (1986).
14. Ishihara, T., Eguchi, K., and Arai, H., *Chem. Lett.* **1986,** 1695 (1985).
15. Arai, H., and Tominaga, K., *J. Catal.* **43,** 131 (1976).
16. Tiep, L. V., Tardy, M. B., Bugli, G., Djega-Mariadassou, G., Che, M., and Bond, G. C., *J. Catal.* **99,** 449 (1986).
17. Narita, T., Miura, H., Sugiyama, K., Matsuda, T., and Gonzalez, R. D., *J. Catal.* **103,** 492 (1987).
18. Joyner, R. W., Pendry, J. B., Soldin, D. K., and Tennison, S. R., *Surf. Sci.* **138,** 84 (1984).
19. Huizinga, T., van't Blik, H. F. J., Vis, J. C., and Prins, R., *Surf. Sci.* **135,** 580 (1983).
20. Pauling, L. "Nature of the Chemical Bond," 3rd ed., Cornell Univ. Press, Ithaca, NY, 1960.
21. Sanderson, R. T. "Chemical Bonds and Bond Energy." Academic Press, New York, 1976.
22. Little, E. J., and Jones, M. M., *J. Chem. Educ.* **37,** 231 (1960).
23. Peri, J. B., *J. Phys. Chem.* **78,** 588 (1974).
24. Gonzalez, R. D., and Miura, H. *J. Catal.* **77,** 338 (1982).
25. Raupp, G. B., and Dumesic, J., *J. Catal.* **95,** 587 (1985).